

## Surface defects and their influence on structural and photoluminescence properties of CdWO<sub>4</sub>:Eu<sup>3+</sup> nanocrystals

Qilin Dai, Hongwei Song, Guohui Pan, Xue Bai, Hui Zhang et al.

Citation: *J. Appl. Phys.* **102**, 054311 (2007); doi: 10.1063/1.2773639

View online: <http://dx.doi.org/10.1063/1.2773639>

View Table of Contents: <http://jap.aip.org/resource/1/JAPIAU/v102/i5>

Published by the [American Institute of Physics](#).

---

### Related Articles

Plasmon-induced near-infrared electrochromism based on transparent conducting nanoparticles: Approximate performance limits

*Appl. Phys. Lett.* **101**, 071903 (2012)

Quantum mechanical study of plasmonic coupling in sodium nanoring dimers

*Appl. Phys. Lett.* **101**, 061906 (2012)

Strong two-photon fluorescence enhanced jointly by dipolar and quadrupolar modes of a single plasmonic nanostructure

*Appl. Phys. Lett.* **101**, 051109 (2012)

Observation of intermediate bands in Eu<sup>3+</sup> doped YPO<sub>4</sub> host: Li<sup>+</sup> ion effect and blue to pink light emitter

*AIP Advances* **2**, 032119 (2012)

Silver nanoclusters decorated diamond thin film as a substrate for surface-enhanced Raman scattering

*AIP Advances* **2**, 032102 (2012)

---

### Additional information on J. Appl. Phys.

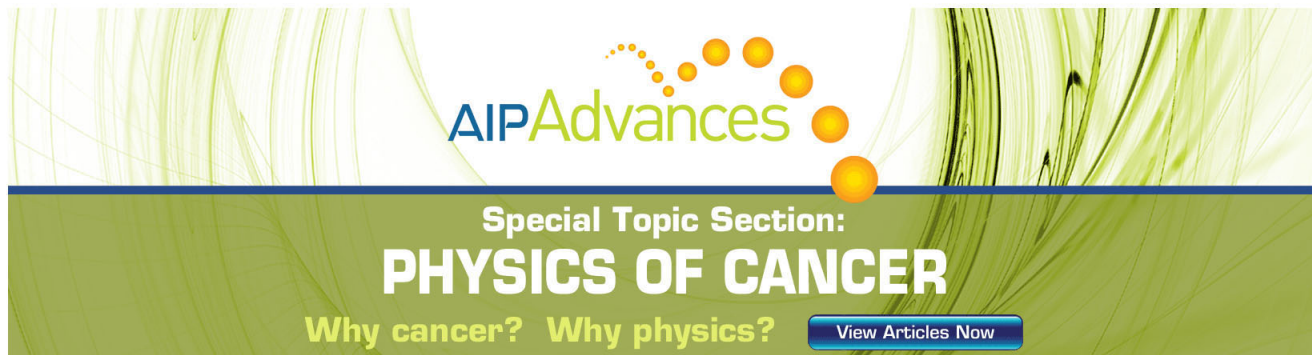
Journal Homepage: <http://jap.aip.org/>

Journal Information: [http://jap.aip.org/about/about\\_the\\_journal](http://jap.aip.org/about/about_the_journal)

Top downloads: [http://jap.aip.org/features/most\\_downloaded](http://jap.aip.org/features/most_downloaded)

Information for Authors: <http://jap.aip.org/authors>

## ADVERTISEMENT



**AIP Advances**

Special Topic Section:  
**PHYSICS OF CANCER**

Why cancer? Why physics? [View Articles Now](#)

# Surface defects and their influence on structural and photoluminescence properties of $\text{CdWO}_4\text{:Eu}^{3+}$ nanocrystals

Qilin Dai

*Key Laboratory of Excited State Physics, Changchun Institute of Optics, Fine Mechanics and Physics, Chinese Academy of Sciences, Changchun 130033, People's Republic of China and Graduate School of Chinese Academy of Sciences, 16 Easter Nan-Hu Road, Changchun 130033, People's Republic of China*

Hongwei Song<sup>a)</sup>

*Key Laboratory of Excited State Physics, Changchun Institute of Optics, Fine Mechanics and Physics, Chinese Academy of Sciences, Changchun 130033, People's Republic of China, Graduate School of Chinese Academy of Sciences, 16 Easter Nan-Hu Road, Changchun 130033, People's Republic of China, and State Key Laboratory of Integral Optoelectronics, College of Electronic Science and Engineering, JiLin University, Changchun 130012, China*

Guohui Pan, Xue Bai, Hui Zhang, Ruifei Qin, Lanying Hu, Haifeng Zhao, Shaozhe Lu, and Xinguang Ren

*Key Laboratory of Excited State Physics, Changchun Institute of Optics, Fine Mechanics and Physics, Chinese Academy of Sciences, Changchun 130033, People's Republic of China and Graduate School of Chinese Academy of Sciences, 16 Easter Nan-Hu Road, Changchun 130033, People's Republic of China*

(Received 24 April 2007; accepted 9 July 2007; published online 14 September 2007)

$\text{CdWO}_4\text{:Eu}^{3+}$  nanocrystals were prepared by the hydrothermal method at different  $p\text{H}$  values ( $p\text{H}=4, 7.5, \text{ and } 10$ ) and annealed at different temperatures. Their structural and photoluminescence properties were systemically studied. The studies on electron spin resonance and Fourier-transfer infrared absorption spectra demonstrated that at least two kinds of surface defects were involved, the surface dangling bonds of transition metals and the surface adsorption of the  $\text{OH}^-$  and  $\text{CO}_3^{2-}$  groups. The surface adsorption in the  $p\text{H}=10$  sample increased considerably, which led the surface dangling bonds to decrease and even to disappear. Due to the existence of surface defect states, especially the surface dangling bonds, tungstates at two symmetry sites were formed, the normal site and the perturbed site locating at/near the surface. The former tungstates located at high energy side ( $\sim 290$  nm) in the excitation bands and emitted blue-green photons, while the latter located at low energy ( $\sim 340$  nm) and emitted red photons. They can both effectively transfer the energies to  $\text{Eu}^{3+}$  ions, generating red  ${}^5D_0\text{-}{}^7F_J$  transitions. As the nanocrystalline powders were annealed, colorations appeared and evolved with temperature, while the surface dangling bonds and surface adsorption gradually disappeared. The defect states had great and complicated influence on luminescence efficiency, luminescent stability, and temperature-stability of tungstates and  $\text{Eu}^{3+}$  ions. © 2007 American Institute of Physics. [DOI: 10.1063/1.2773639]

## I. INTRODUCTION

It is known that tungstate is a very important family of inorganic material that has a high potential application in various fields, such as photoluminescence,<sup>1</sup> microwave applications,<sup>2</sup> optical fibers,<sup>3</sup> scintillator materials,<sup>4</sup> and so on. As a self-activating phosphor, tungstate has some advantages, e.g., high chemical stability, high x-ray absorption coefficient, high light yield, and low afterglow to luminescence.<sup>5</sup> There exist two types of structure in tungstates: wolframite and scheelite. Cadmium tungstate has the wolframite structure that is monoclinic with space group  $P2_1/c$ . The luminescent properties of cadmium tungstate have been extensively investigated because it is a widely used scintillation crystal.<sup>1,6-8</sup> Its luminescence originates from two parts; one is the intrinsic structure—the charge transfer

from excited  $2p$  orbits of  $\text{O}^{2-}$  to the empty orbits of the central  $\text{W}^{6+}$  ions, and the other is the structural defects. There are few reports about these kinds of defects; some authors ascribe that to the transitions in a tungstate group, which lack one oxygen ion.<sup>9</sup> As for  $\text{Eu}^{3+}$  ions doped tungstates, tungstates emit blue-green lights themselves under ultraviolet (UV) excitation. At the same time, tungstates may also effectively transfer energy to  $\text{Eu}^{3+}$  ions, generating strong red emissions.<sup>10,11</sup> Therefore,  $\text{Eu}^{3+}$  ions doped tungstates also become potential white-light phosphors.

The studies on luminescence properties of nanosized phosphors are attracting current interests; because it is significant not only for applications but also for essential understanding of nanocrystals, such as confinement effect, surface effect, etc. Among them, some rare earth doped nanophosphors have attracted particular attention,<sup>12-14</sup> because the corresponding bulk materials have large practical applications in lighting and display,<sup>15,16</sup> etc. In addition, some rare

<sup>a)</sup>Author to whom correspondence should be addressed. FAX: 86-431-86176320. Electronic mail: hwsong2005@yahoo.com.cn

earth ions such as  $\text{Eu}^{3+}$  and  $\text{Sm}^{3+}$  may act as common activators to detect local environments<sup>17</sup> due to their supersensitive  $f-f$  transitions. Up to now, a great number of rare earth doped nanosized phosphors have been prepared and studied,<sup>18–20</sup> including tungstates. It is expected that in the nanosized phosphors the luminescent quantum yield as well as the resolution of display be improved considerably. However, due to a number of surface defects involved in nanosized phosphors, usually the quantum yield of nanosized phosphors is rather lower than that of the corresponding bulk materials. Therefore, defect states including structure and surface defects play a very important role in the luminescence of rare earth doped nanosized tungstate. It is important to study the defect states and their influence on photoluminescence in this kind of material. In the past few years, there were quite a few articles about tungstate; however, among them few articles were about the structure and surface defects in nanosized tungstate. In this article we obtained  $\text{CdWO}_4\cdot\text{Eu}^{3+}$  nanocrystals by the hydrothermal method under different  $p\text{H}$  values and annealed at different temperatures and systemically studied their structural and photoluminescence properties by different methods, especially, the relationship between the defect states (including inner and surface defects) and photoluminescence. It is interesting to observe that the excitation and emission spectra have a close relationship with the defect states. The luminescent stability and temperature stability strongly depend on defect states too. It is believed that this study is not only helpful for the understanding of the influence of defect states on photoluminescence in nanocrystalline  $\text{CdWO}_4\cdot\text{Eu}^{3+}$  itself, but also helpful for the understanding of that in the other hydrothermal products.

## II. EXPERIMENTS

### A. Sample preparation

Cadmium tungstate ( $\text{CdWO}_4$ ) nanocrystals were prepared by the reaction of  $(\text{CH}_3\text{COO})_2\text{Cd}$  and  $(\text{CH}_3\text{COO})_3\text{Eu}$  as well as  $\text{Na}_2\text{WO}_4$  for 12 h at a certain temperature (160 °C) and different  $p\text{H}$  values. In a typical procedure,  $(\text{CH}_3\text{COO})_3\text{Eu}\cdot 4\text{H}_2\text{O}$ ,  $(\text{CH}_3\text{COO})_2\text{Cd}\cdot 2\text{H}_2\text{O}$ , and  $\text{Na}_2\text{WO}_4\cdot 2\text{H}_2\text{O}$  were dissolved in de-ionized water, respectively. Then the former two solutions were mixed together [1 mmol  $(\text{CH}_3\text{COO})_2\text{Cd}$  and 0.02 mmol  $(\text{CH}_3\text{COO})_3\text{Eu}$ ] and then appropriate  $\text{Na}_2\text{WO}_4$  (1 mmol) was added with vigorous stirring. The  $p\text{H}$  value ( $p\text{H}=4, 7.5, 10$ ) of the mixed solution was adjusted dropwise with  $\text{CH}_3\text{COOH}$  or  $\text{NaOH}$  solution. After that, the solution was added into a Teflon-lined stainless steel autoclave of 50.0 ml capacity. The autoclave was kept at 160 °C for 12 h. Afterwards the autoclave was cooled to room temperature gradually. Then the white precipitate was collected and washed with de-ionized water several times. The solid was heated at 80 °C and dried under vacuum for 2 h, finally the white powders of  $\text{CdWO}_4\cdot\text{Eu}^{3+}$  (the doping concentration was 2 mol %) were obtained.

## B. Measurements

Field emission scanning electron microscopy (FE-SEM) was taken on a HITACHI S-4800 electron microscope. X-ray diffraction (XRD) data were collected on a Rigaku D/max-rA x-ray diffractometer using a Cu target radiation source. The UV-visible (Vis) absorption spectra were recorded at an UV-Vis-near infrared scanning spectrophotometer (SHI-MADZU). In the measurement, the powder was dispersed in the ethanol through ultrasonic to get the corresponding suspension. The Fourier-transform infrared (FTIR) absorption spectra were measured by a FTS3000 FTIR spectrometer. The electron spin resonance (ESR) spectra were measured by a GAES-FE3AX ESR spectrometer at room temperature. It was with a central magnetic field strength of 3363 G, scanning scope of 5000 G, multiplying factor of 5000 G, and was calibrated with 1,1-Diphenyl-2-picrylhydrazyl (DPPH). Emission and excitation spectra were recorded at room temperature using a Hitachi F-4500 spectrophotometer equipped with a continuous 150 W Xe-arc lamp. For comparison of different samples, the emission spectra were measured at a fixed bandpass of 0.2 nm with the same instrument parameters (2.5 nm for the excitation slit, 2.5 nm for the emission slit, and 700 V for the photomultiplier tube voltage). In the experiments of spectral change induced by UV light irradiation, the monochromic light separated from the same Xe-arc lamp was used as the irradiation source, which was with a slit of 10 nm. In the measurements of temperature dependence of emission intensity, the samples were put into a liquid nitrogen cycling system, in which the temperature varied from 77 to 300 K. The 325-nm light came from a He-Cd laser was used for excitation. The spectra were recorded by a UV-Laboratory Raman infinity with a resolution of  $2\text{ cm}^{-1}$ . In the measurements of temperature-dependent emission spectra, the samples were put into a helium-gas cycling system where the temperature varied from 10 to 300 K. A 266-nm laser generated from a pulsed Nd:yttrium-aluminum-garnet (YAG) laser combined with a fourth-harmonic-generator was used as pumping source, with a linewidth of  $0.2\text{ cm}^{-1}$ , pulse duration of 10 ns, and repetition frequency of 10 Hz. A Rhodamine 6 G dye pumped by the same Nd:YAG laser was used as the frequency-selective excitation source. A Spex 1403 spectrometer and a boxcar integrator were used to record the emission spectra. The experiments of frequency-selective excitation and fluorescence dynamics were performed at 77 K, in which the samples were put into a liquid nitrogen system.

## III. STRUCTURAL PROPERTIES

### A. Morphology and crystalline phase

Figure 1 shows FE-SEM images of  $\text{CdWO}_4\cdot\text{Eu}^{3+}$  nanocrystals prepared at different  $p\text{H}$  values and annealed at different temperatures. The powders prepared at  $p\text{H}=4$  yield nanorods with diameter of  $\sim 30$  nm and length of  $\sim 100$  nm. As the  $p\text{H}$  value was adjusted to 7.5, they had an average diameter of  $\sim 100$  nm and length of  $\sim 300$  nm. The powders prepared at  $p\text{H}=10$  yield nanoparticles, with an average diameter of  $\sim 50$  nm. After annealing at 600 °C, the size and morphology of the nanocrystalline powders nearly

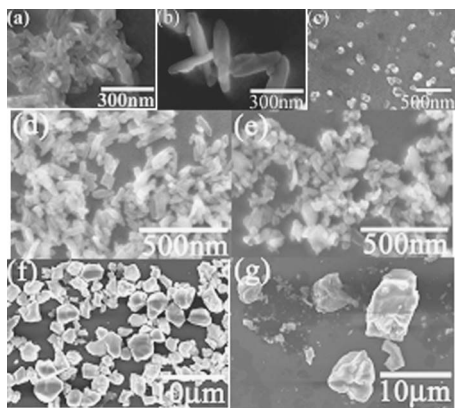


FIG. 1. FE-SEM images of the  $\text{CdWO}_4:\text{Eu}^{3+}$  samples prepared at (a)  $p\text{H}=4$ , (b)  $p\text{H}=7.5$ , (c)  $p\text{H}=10$ , (d) the sample for  $p\text{H}=4$  annealed at  $600^\circ\text{C}$  for 2 h, (e) the sample for  $p\text{H}=10$  annealed at  $600^\circ\text{C}$  for 2 h, (f) the sample for  $p\text{H}=4$  annealed at  $1100^\circ\text{C}$  for 2 h, and (g) the sample for  $p\text{H}=10$  annealed at  $1100^\circ\text{C}$  for 2 h.

did not change, for both the  $p\text{H}=4$  and 10 samples. After annealing at  $1100^\circ\text{C}$  for 2 h, the nanocrystalline powders prepared both at  $p\text{H}=4$  and  $p\text{H}=10$  aggregate together, forming irregular particles with a rough size of  $2\ \mu\text{m}$ . The particle distribution for the  $p\text{H}=4$  powders is relatively homogenous. Some small nanoparticles still exist in the  $p\text{H}=10$  particles.

Figure 2 shows the XRD patterns of  $\text{CdWO}_4:\text{Eu}^{3+}$  powders prepared at different  $p\text{H}$  values in comparison to the standard card (JCPDS No. 80-0139). It can be seen that the crystal structures of all the samples belong to the pure monoclinic phase. Estimated according to the Scherrer equation, the average crystalline sizes of the powders for  $p\text{H}=4, 7.5, 10$  are  $\sim 30$ ,  $\sim 150$ , and  $\sim 30$  nm, respectively, which are nearly identical with those observed by FE-SEM images.

## B. UV-Vis and FTIR absorption spectra

Figure 3(a) shows the UV-VIS absorption spectra for the  $p\text{H}=4$  samples annealed at different temperatures, while Fig. 3(b) depicts those for the  $p\text{H}=10$  samples. There appears an extra weaker absorption band for the samples annealed at  $400$ ,  $600$ , and  $900^\circ\text{C}$ , locating at  $\sim 430$  nm, as shown in the inset of Fig. 3(b). It should be noted that the samples  $p\text{H}=10$  and annealed at  $400$ ,  $600$ , and  $900^\circ\text{C}$  were light yellow, which is in consistent with their absorption spectra. The other powders were white. The band gap absorption of

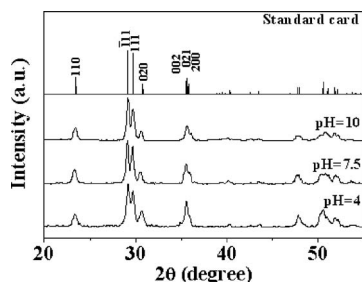


FIG. 2. XRD pattern of  $\text{CdWO}_4:\text{Eu}^{3+}$  powders prepared at  $160^\circ\text{C}$ , under different  $p\text{H}$  values in comparison to the standard card.

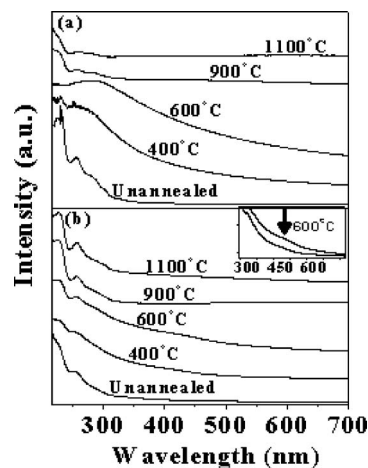


FIG. 3. The absorption spectra for the samples (a)  $p\text{H}=4$  and (b)  $p\text{H}=10$  annealed at different temperatures.

$\text{CdWO}_4$  film is  $3.7\text{--}3.8$  eV. Different references gave a little different values.<sup>5,21</sup> The band at  $\sim 430$  nm ( $\sim 2.9$  eV) should be assigned to some color centers caused by defects forming from annealing the samples instead of band gap absorption.

Figure 4 shows the FTIR spectra for different samples normalized by the value of the peak at  $835\ \text{cm}^{-1}$ . According to the literature, the peaks located at  $\sim 835\ \text{cm}^{-1}$  are assigned to the  $\nu_{\text{as}}$  stretch of the  $\text{WO}_2$  terminal bonds<sup>22</sup> in tungstate groups, the bands at  $\sim 1625$  and  $\sim 3500\ \text{cm}^{-1}$  are assigned to the  $-\text{OH}$  bending and stretching modes, respectively. From the spectra it is obvious that the intensity of  $-\text{OH}$  modes for the  $p\text{H}=10$  sample is higher than that for the  $p\text{H}=4$  sample, which should be caused by intensive existent of OH bonds in the basic precursor solution. The band at  $\sim 1450\ \text{cm}^{-1}$  in the  $p\text{H}=7.5$  and 10 samples is assigned to the vibration of  $\text{CO}_3^{2-}$ . In the  $p\text{H}=4$  sample the band could not be identified. The  $\text{CO}_3^{2-}$  group originated from the  $\text{CO}_2$  in the air and the solution was acidic for  $p\text{H}=4$  thus rather less even none  $\text{CO}_3^{2-}$  would exist in the solution.

## C. ESR spectra

To further reveal the structural defects involved in the nanocrystalline powders, the ESR experiments were performed at room temperature in various samples. Figure 5 shows the EPR spectra in different samples. No signal appears for the  $p\text{H}=10$  sample, whereas two kinds of signals exhibit the  $p\text{H}=4$ . One is relatively strong, broad, and un-

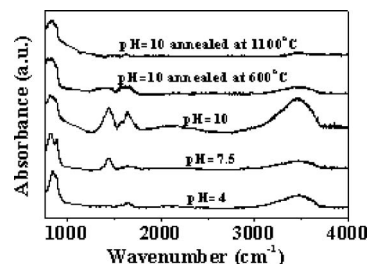


FIG. 4. The FTIR spectra for different samples, normalized by the value of the peak at  $835\ \text{cm}^{-1}$  for  $p\text{H}=4$ ,  $p\text{H}=7.5$ ,  $p\text{H}=10$ , the sample for  $p\text{H}=10$  annealed at  $600^\circ\text{C}$  for 2 h, and the sample for  $p\text{H}=10$  annealed at  $1100^\circ\text{C}$  for 2 h.

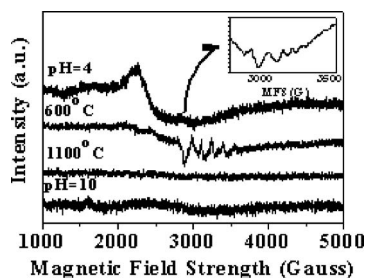


FIG. 5. ESR spectra of the following four samples:  $pH=4$ , annealed the sample  $pH=4$  600 °C for 2 h, annealed the sample  $pH=4$  1100 °C for 2 h, and  $pH=10$ . The inset was the location-enlarged pattern of  $pH=4$  as the arrow marked.

symmetrical, located in the range of 2000–4000 G. The other is relative weak and displays five sharp peaks, located at 2989, 3113, 3236, 3400, and 3523 G, respectively, as shown in the inset. In the sample annealed at 600 °C, only the sharp peaks appear and their intensities become stronger in comparison to the untreated samples. After being annealed at 1100 °C, the sharp peaks disappear. Some positions of the sharp ESR peaks (measured at room temperature) are identical to that reported by other authors that measured at low temperature,<sup>23</sup> thus they probably come from the Mo element. In the starting material  $Na_2WO_4$  contains Mo 0.001%. As for the broader and unsymmetrical signal, its origin is not very clear. Judged according to its shape, it may originate from dangle bonds of some transition metals.

#### IV. LUMINESCENCE PROPERTIES

##### A. Emission and excitation spectra

Figure 6 (left part) shows the excitation spectra for different  $pH$  samples. In the spectra, the bands extending from 200 to 400 nm are dominant. The sharp line assigned to the  ${}^7F_0-{}^5L_6$  transition of  $Eu^{3+}$  can also be observed. The broadbands can be decomposed into two Gaussian components, A and B. The location of peak A is around 290 nm, while that of peak B is around 340 nm. The two peaks have a little shift (<10 nm) in different samples. According to the literature, the charge transfer band for  $Eu^{3+}$  in the tungstate centers is around 250 nm.<sup>24</sup> Peak A is assigned to transitions of tungstate at normal lattice sites.<sup>9,24</sup> The low energy side line (peak B) is also observed in the other literature, which is generally attributed to tungstate transitions at perturbed sites. These perturbed sites might be tungstate ions next to either

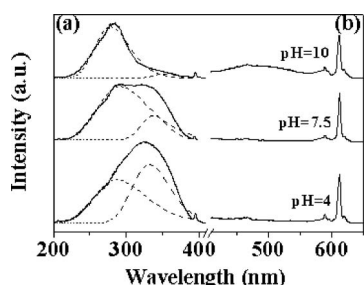


FIG. 6. Room-temperature excitation spectra (left part) ( $\lambda_{em}=612$  nm) and emission spectra (right part) ( $\lambda_{ex}=290$  nm) of  $Eu^{3+}$  in  $CdWO_4:Eu^{3+}$  powders prepared at different  $pH$  values.

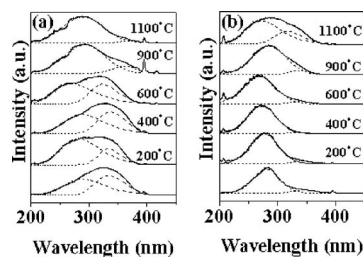


FIG. 7. The excitation spectra for different samples annealed for 2 h at different temperatures: (a)  $pH=4$  and (b)  $pH=10$ .

chemical or structural defects and thus had a different symmetry and crystal field strength than tungstate ions at normal lattice site. Some authors ascribe it to the transitions in the tungstate group which lack one oxygen ion.<sup>9</sup>

The corresponding emission spectra under the excitation of the same continuous Xe lamp are shown in Fig. 6 (right part). In the  $pH=10$  samples, the emission bands peaking around 478 nm can be clearly observed, which are assigned to the transitions of normal tungstate groups.<sup>9</sup> In the samples of  $pH=4$  and 7.5, the peak at 478 nm is absent. It is evident that as the  $pH$  value increases the luminescence of tungstate becomes strong.

Figure 7 shows the excitation spectra of the different  $pH$  series annealed at different temperatures. From the dissolved spectra of Fig. 7(a) it can be seen that for the  $pH=4$  sample the relative contribution of peak B to peak A increases with annealing temperature. As the annealing temperature goes beyond 600 °C, it begins to drop. From Fig. 7(b) it is obvious that for the  $pH=10$  sample the relative contribution of the two peaks, A and B, has only a little variation with annealing temperature. The contribution of peak A is dominant all the time. It is interesting to note that in the samples of  $pH=4$  and 10 annealed at 1100 °C (bulk), the line shapes of excitation spectra are nearly the same.

The emission intensity of  $Eu^{3+}$  for the  $pH=4$  and  $pH=10$  samples annealed at different temperatures are shown in Fig. 8. In the annealed samples the particle size increases gradually with increasing temperature, thus the surface defects acting as nonradiative channels decrease, which should lead to the increase of emission intensity. However, for the  $pH=10$  series, the intensity as a function of annealing temperature does not increase as expected in the range of 400–900 °C, it even becomes lower than the untreated sample. This is attributed to the influence of colorations that exist in these samples, which can capture the excited energy of the tungstates.

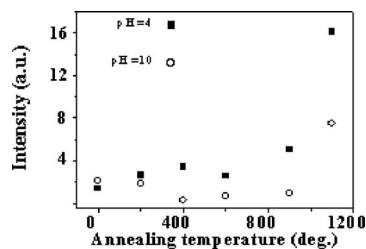


FIG. 8. The intensity varied with different annealing temperatures for  $pH=4$  and  $pH=10$  ( $\lambda_{ex}=290$  nm).

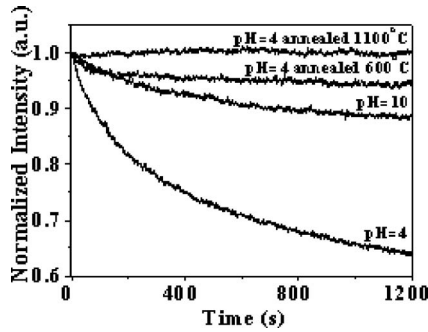


FIG. 9. Dependence of emission intensity at 612 nm on irradiation time ( $\lambda_{\text{ex}}=325$  nm) for the following samples: Annealed the sample  $pH=4$  1100 °C for 2 h, annealed the sample  $pH=4$  600 °C for 2 h,  $pH=10$ , and  $pH=4$ .

## B. UV-light irradiation induced intensity change

The dependence of emission intensity of  $\text{Eu}^{3+}$  on irradiation time under 325-nm excitation was measured and compared in different samples, as shown in Fig. 9. As mentioned in Sec. III, as the samples were annealed, the particle size gradually increased, the surface dangling bonds and the surface adsorption gradually decreased. The UV-light irradiation induced intensity change should be related to surface defects. The UV-irradiation induced spectral change was also observed in the other  $\text{Eu}^{3+}$  doped nanomaterials.<sup>14</sup> The essential of this process is the optical rearrangements of local environments surrounding  $\text{Eu}^{3+}$  ions. Note that the light-irradiation experiments were also performed under the excitation of 280-nm light, which demonstrated the same fact.

## C. Temperature dependence of photoluminescence

The temperature-dependent photoluminescence properties in the different samples ( $pH=4$  and  $pH=10$ ) were studied under excitation of the 266- and 325-nm lasers, respectively, which correspond to two different excitation peaks in the excitation spectra, tungstate and perturbed tungstate groups. The emission spectra at different temperatures (10–200 K) under the excitation of the 266-nm pulsed laser are shown in Fig. 10. In the emission spectra, both the blue-green emission bands originate from tungstate groups and the red emissions of  ${}^5D_0-{}^7F_2$  appear, like those excited by the continuous lights shown in Fig. 6. Differently, under the excitation of the pulsed laser the intensity for the band emissions surpasses that for  $\text{Eu}^{3+}$ . In fact, the relative intensity of the band emissions to  $\text{Eu}^{3+}$  should vary with delay time because the band emissions have a shorter lifetime than that for  $\text{Eu}^{3+}$ . In the studied range, the photoluminescence of  ${}^5D_0-{}^7F_2$  has only a little variation with temperature, for both the two powders ( $pH=4$  and  $pH=10$ ), and thus it is normalized. Figure 10(c) shows dependence of relative luminescence intensity of tungstate to  $\text{Eu}^{3+}$  on temperature. It can be seen obviously that the temperature stability of the photoluminescence for the tungstate in the  $pH=10$  sample is much better than that in the  $pH=4$ .

Figure 11 shows fluorescence spectra at various temperatures under the 325-nm excitation and Fig. 12 shows the dependence of  $\text{Eu}^{3+}$  and tungstate group emission intensity

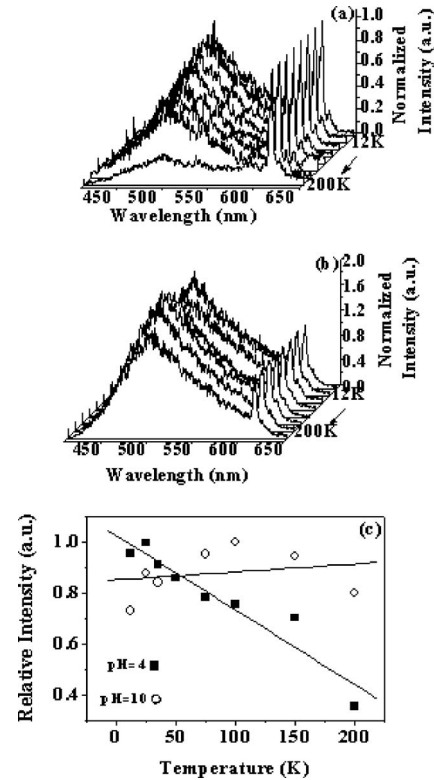


FIG. 10. The emission spectra measure at different temperatures from 12 to 200 K pumped by 266 nm laser for different samples (a)  $pH=4$ , (b)  $pH=10$ , normalized by the intensity of  $\text{Eu}^{3+}$ , and (c) the relative luminescence intensity of tungstate to  $\text{Eu}^{3+}$  varied with temperatures for different  $pH$  values.

on temperature. The intensity as a function of temperature is well fitted by the well-known thermal activation function<sup>25</sup>

$$I(T) = \frac{I_0}{1 + \alpha e^{E_A/k_B T}}, \quad (1)$$

where  $I_0$  is the emission intensity at 0 K,  $\alpha$  is the proportional coefficient,  $E_A$  is the thermal activation energy,  $k_B$  is

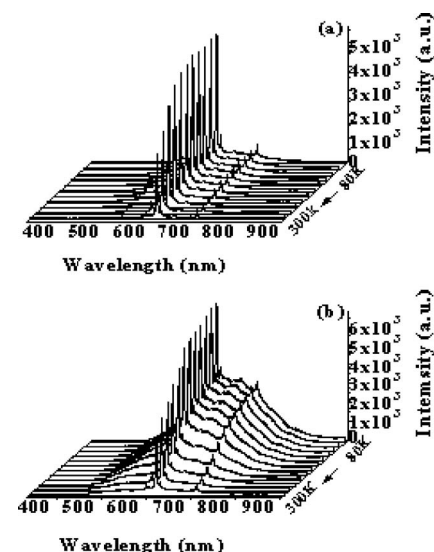


FIG. 11. The emission spectra measured at different temperatures from 80 to 300 K excited by a 325-nm He-Cd laser for different samples (a)  $pH=4$  and (b)  $pH=10$ .

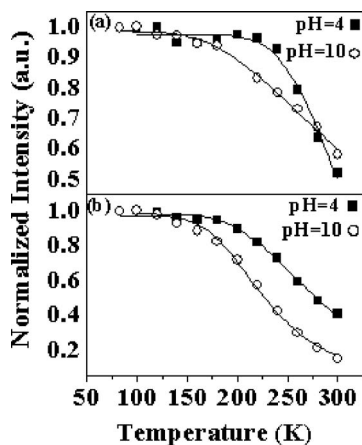


FIG. 12. Dependence of  $\text{Eu}^{3+}$  and tungstate group emission intensity on temperature in samples  $\text{pH}=4$  and  $\text{pH}=10$  (a)  $\text{Eu}^{3+}$  (b) tungstate group ( $\lambda_{\text{ex}}=325$  nm).

Boltzmann's constant, and  $T$  is the absolute temperature. The values of  $I_0$ ,  $\alpha$ , and  $E_A$  obtained by fitting are listed in Table I. It is obvious that for the luminescence of  $\text{Eu}^{3+}$ , the temperature stability for the  $\text{pH}=4$  sample is more stable than that for the  $\text{pH}=10$ .

#### D. Frequency-selective excitation and site symmetry

Figures 13(a) and 13(b) show, respectively,  ${}^7F_0-{}^5D_0$  excitation spectra monitoring different  ${}^5D_0-{}^7F_2$  sites, and the  ${}^5D_0-{}^7F_2$  emission spectra selectively exciting  ${}^7F_0-{}^5D_0$  transitions. In Fig. 13(a), every curve can be decomposed into two excitation peaks. The observation of two  ${}^7F_0-{}^5D_0$  excitation peaks indicates that there exist two luminescent symmetry sites, which are labeled as site  $P$  and site  $Q$ , respectively. According to our previous results,<sup>26</sup> the emission of  $\text{Eu}^{3+}$  at symmetry site  $P$  corresponds to the photoluminescence of  $\text{Eu}^{3+}$  at the surface site, while that at site  $Q$  corresponds to the luminescence at the inner site. According to the linewidth, it can be concluded that the local environments surrounding  $\text{Eu}^{3+}$  at the surface site for the  $\text{pH}=10$  sample are more disordered than that for the  $\text{pH}=4$ , which could be attributed to decreased particle size.

The fluorescence decay dynamics were also measured by site-selective excitation, at 77 K and room temperature. The corresponding exponential fluorescent lifetimes measured in different samples and at different conditions are listed as Table II. Accordingly, several conclusions can be drawn: (1) The fluorescence lifetime for  $\text{Eu}^{3+}$  locating at the surface site is shorter than that at the inner site; (2) As the temperature varied, the fluorescence lifetime at the surface site nearly does not change, while that at the inner site decreases to

TABLE I. The fitting parameters  $\alpha$  and  $E_A$  according to Eq. (1).

	$\text{Eu}^{3+}$		Perturbed tungstate group	
	$\text{pH}=4$	$\text{pH}=10$	$\text{pH}=4$	$\text{pH}=10$
$I_0$	$0.97 \pm 0.01$	$0.98 \pm 0.07$	$0.98 \pm 0.01$	$0.97 \pm 0.01$
$\alpha$	$15095.3 \pm 5497.7$	$24.8 \pm 0.3$	$365.2 \pm 2.8$	$826.4 \pm 94.0$
$E_A$ (meV)	$250.2 \pm 7.9$	$94.1 \pm 0.1$	$142.6 \pm 0.5$	$132.7 \pm 0.4$

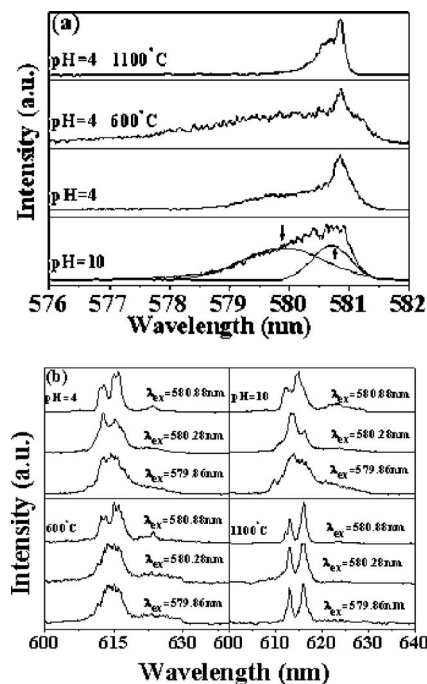


FIG. 13. (a)  ${}^7D_0-{}^5D_0$  excitation spectra monitoring different  ${}^5D_0-{}^7F_2$  sites at 77 K, for the following four samples:  $\text{pH}=4$ ,  $\text{pH}=10$ , the sample for  $\text{pH}=4$  annealed at 600 and 1100 °C for 2 h. (b)  ${}^5D_0-{}^7F_2$  emission spectra selectively exciting  ${}^7F_0-{}^5D_0$  transitions at 77 K in samples:  $\text{pH}=4$ ,  $\text{pH}=10$ , the sample for  $\text{pH}=4$  annealed at 600 and 1100 °C for 2 h.

some content; (3) The fluorescence lifetime for  $\text{Eu}^{3+}$  in the sample prepared at  $\text{pH}=4$  is longer than that prepared at  $\text{pH}=10$ .

#### E. Relationship between surface defects and photoluminescence

The goal of this article is to reveal the relationship between the luminescence property and structure of nanocrystalline  $\text{CdWO}_4$ , in which various techniques have been used. Because the experimental methods and results both are very complicated, the main results concluded by the different techniques are listed in Table III. In the nanocrystalline  $\text{CdWO}_4$  powders before annealing, at least two kinds of surface defects have been involved, the dangling bonds and surface adsorption, which can be identified by the ESR and FTIR spectra, respectively. Although the detailed origins of the dangling bonds cannot be clearly distinguished, it can be roughly estimated that they originate from some transition metal with unpaired electrons. Due to the fact that the ESR signals disappear after annealing (the nanoparticles aggregated to microsized particles) and the ESR signals are rather weak in the samples highly containing surface absorption groups, they are attributed to the surface dangling bonds. Analyzed according to the components of the powders, it is possible that the surface dangling bonds are partly caused by unpaired electrons from tungsten. Of course, the dangling bonds may also be caused by some metal impurities, such as Mo. It should be pointed out that the forming of surface defects depends mainly on the preparation conditions ( $\text{pH}$  value). For the samples prepared at different conditions, the particle shape and size change, leading to the variation of

TABLE II. The lifetime for the samples  $pH=4$  and  $pH=10$  measured at room temperature and 77 K.  $\tau$  was the decay time constant of  $\text{Eu}^{3+}$ .

Samples	$\lambda_{\text{ex}}$ (nm)	$\lambda_{\text{em}}=612$ nm		$\lambda_{\text{em}}=615$ nm	
		$\tau$ ( $\mu\text{s}$ ) (77 K)	$\tau$ ( $\mu\text{s}$ ) (300 K)	$\tau$ ( $\mu\text{s}$ ) (77 K)	$\tau$ ( $\mu\text{s}$ ) (300 K)
$pH=4$	579.86 (surface)	$396.4 \pm 0.7$	$376.9 \pm 0.5$	$412.9 \pm 0.6$	$406.0 \pm 0.5$
	580.88 (inner)	$615.5 \pm 0.7$	$512.2 \pm 0.7$	$629.5 \pm 0.6$	$516.0 \pm 0.6$
$pH=10$	579.86 (surface)	$365.5 \pm 0.4$	$348.8 \pm 0.6$	$385.8 \pm 0.4$	$373.1 \pm 0.7$
	580.88 (inner)	$535.7 \pm 0.6$	$463.9 \pm 0.8$	$521.0 \pm 0.4$	$450.3 \pm 0.6$

surface to volume ratio, however, the variation degree is not much, which should have only a little influence on the forming of defect states.

In the  $pH=4$  sample, more surface dangling bonds exist. Generally, tungsten atoms coordinate with the oxygen forming  $\text{WO}_6$  structure. As the oxygen is insufficient, tungsten atoms might also coordinate with an oxygen forming perturbed tungstate group lack one oxygen ion ( $\text{WO}_5$ ), which is supported by the appearance of the 340-nm peak in excitation spectra. This also means that on the surface a number of oxygen vacancies exist, which display a positive charge and can trap electrons or the energy of electrons. In this case, the near surface of the nanosized particle is particularly unstable. The local environments for the  $\text{Eu}^{3+}$  ions in the near surface are easily rearranged by UV irradiation, leading to the change of excitation intensity. A special case is that the energies of excited state tungstates are captured by oxygen vacancies during migration, instead of  $\text{Eu}^{3+}$  ions. As the charge negative groups of  $\text{OH}^-$  and  $\text{CO}_3^{2-}$  adsorb, the surface dangling bonds decrease or disappear, as a consequence, the photoluminescence of  $\text{Eu}^{3+}$  become more stable. In some literature, the surface adsorption groups of  $\text{OH}^-$  and  $\text{CO}_3^{2-}$  have a negative influence on the photoluminescence because they can act as nonradiative relaxation channels due to their vibration modes with large phonon energy. Here this effect

should still occur. In addition, in the sample containing more surface dangling bonds ( $pH=4$ ), the transitions originate from normal tungstate that decreased considerably, suggesting that an effective energy transfer occurred between the tungstate and the surface dangling bonds.

## F. Evolution of defect states on annealing temperature

In the absorption spectra (see Fig. 3), it can be observed that the absorption band varies significantly with the annealing temperature, indicating that the structure and the defect states change with the annealing temperature. In the  $pH=10$  sample series, the colorations appear after annealing at 400 and 600 °C. And, the excitation spectra do not change, suggesting that the appearance of colorations do not accompany with the appearance of the perturbed tungstate groups ( $\text{WO}_5$ ). From Fig. 8 it can be observed that after annealing below 600 °C, the surface adsorption of the  $\text{OH}^-$  and  $\text{CO}_3^{2-}$  bonds decrease greatly, which would decrease the nonradiative relaxation channels, however, its photoluminescence does not increase but decrease. It is suggested that the colorations capture the excited energy of the tungstate groups in the annealed samples.

TABLE III. Comparison of experimental results for the nanocrystalline powders prepared at different  $pH$  values.

$pH=4$	$pH=10$	Experiments
Nanorods	Nanoparticles	SEM
Monoclinic phase	Monoclinic phase	XRD
(1) 288-nm band varied with annealing temperature	(1) 288-nm band did not vary	UV-Vis spectra
(2) Color centers did not appear	(2) Color centers appeared after annealing	
Containing less $\text{OH}^-$ , $\text{CO}_3^{2-}$	Containing more $\text{OH}^-$ , $\text{CO}_3^{2-}$	FTIR spectra
Signals appeared	No signal	ESR spectra
340-nm peak appeared (perturbed tungstate group)	340-nm peak nearly disappeared (perturbed tungstate group)	Excitation Spectra of $\text{Eu}^{3+}$
(1) Weaker blue-green emission of tungstate group	(1) Stronger blue-green emission of tungstate group	Emission spectra
(2) Stronger red emission of perturbed tungstate group	(2) Stronger red emission of perturbed tungstate group	
Bad luminescent stability	Better luminescent stability	UV exposure
(1) Better temperature-stability of $\text{Eu}^{3+}$ , perturbed tungstate group	(1) Bad temperature-stability of $\text{Eu}^{3+}$ , perturbed tungstate group	Temperature dependence
(2) Bad temperature-stability of tungstate group.	(2) Better temperature-stability of tungstate group.	
Longer lifetime	Shorter lifetime	Luminescence dynamics



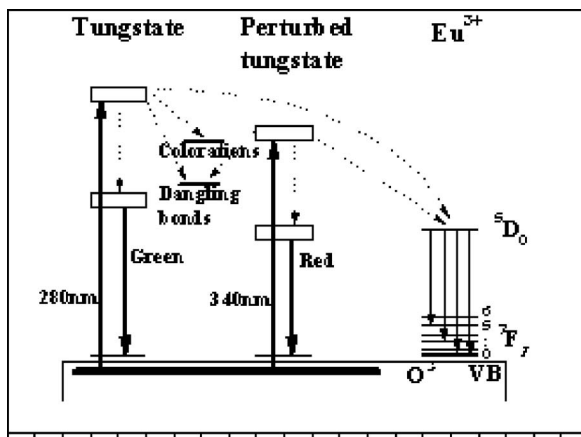


FIG. 14. The schematic of the energy transfer and photoluminescence processes for nanocrystalline  $\text{CdWO}_4:\text{Eu}^{3+}$ .

In the  $p\text{H}=4$  sample, the excitation and the absorption spectra both change with annealing and the tendency of their changes is identical: the excitation and absorption band at the long wavelength side increase with the annealing temperature below  $600^\circ\text{C}$ . This indicates that more perturbed tungstates are formed after annealing and their contribution to the photoluminescence increases. From the SEM images we can know that below  $600^\circ\text{C}$  the shapes of the nanoparticles do not change. Presently, we cannot completely understand how the perturbed tungstates or the color centers formed during the annealing, however, what we can say is that the variation of perturbed tungstates or the color centers is probably related to the surface change of the nanoparticles, because when the annealing temperature increased to  $1100^\circ\text{C}$  and the nanoparticles grew to microsized particles the perturbed tungstates or the color centers nearly disappeared.

According to the earlier discussion, a schematic of the energy transfer and photoluminescence processes for nanocrystalline  $\text{CdWO}_4:\text{Eu}^{3+}$  is given in Fig. 14.

## V. CONCLUSIONS

$\text{CdWO}_4:\text{Eu}^{3+}$  nanorods and nanoparticles were obtained by the hydrothermal method at different  $p\text{H}$  values ( $p\text{H}=4, 7.5,$  and  $10$ ) and annealed at different temperatures. Their photoluminescence properties related with structure and defect states were systemically studied. The results indicate that variation of  $p\text{H}$  values has significant influence on the structure, type, and number of surface defects and thus has great influence on the photoluminescence. Two types of tungstates, the normal and the perturbed, exist in nanocrystalline  $\text{CdWO}_4:\text{Eu}^{3+}$  powders and the ratio of the perturbed structure to the normal structure decreases with increasing  $p\text{H}$  values and also vary with the annealing temperature, which can be concluded according to the excitation spectra.

The  $p\text{H}=10$  sample absorbs more  $\text{OH}^-$  and  $\text{CO}_3^{2-}$  groups in contrast to the  $p\text{H}=4$  sample. These groups combine with surface dangling bonds, leading to the decrease of surface states and surface nonradiative relaxation channels. In the

$p\text{H}=10$  sample, the luminescent stability under the exposure of UV light increases, while the temperature stability of the luminescence decreases in comparison to the  $p\text{H}=4$  sample.

There exist two symmetry sites for the  $^5\text{D}_0-^7\text{F}_2$  emissions of  $\text{Eu}^{3+}$ , inner and surface. The former corresponds to lines with a narrower inhomogeneous width, while the latter corresponds to the lines with a broader width. As the sample is annealed, the relative contribution of the surface site decreases.

## ACKNOWLEDGMENTS

The authors gratefully thank Professor Shihua Huang of the Key Laboratory of Luminescence and Optical Information, Institute of Optoelectronic Technology, Beijing Jiaotong University, Beijing 100044, China for the decomposition of the peaks using Gaussian Function, and thank Dr. E. Elsts and Professor U. Rogulis of the Institute of Solid State Physics, University of Latvia, 8 Kengaraga Str., LV-1063 Riga, Latvia for the helpful discussion on ESR spectra. This work is supported by the National Natural Science Foundation of China (Grant Nos. 10374086 and 10504030) and the Talent Youth Foundation of JiLin Province (Grant No. 20040105).

- <sup>1</sup>L. Bardelli, M. Bini, and P. Bizzeti, Nucl. Instrum. Methods Phys. Res. A **569**, 743 (2006).
- <sup>2</sup>L. G. Van Uitert and S. Preziosi, J. Appl. Phys. **33**, 2908 (1962).
- <sup>3</sup>H. Wang, F. Medina, Y. Zhou, and Q. Zhang, Phys. Rev. B **45**, 10356 (1992).
- <sup>4</sup>K. Tanaka, T. Miyajima, N. Shirai, Q. Zhang, and R. Nakata, J. Appl. Phys. **77**, 6581 (1995).
- <sup>5</sup>Z. Lou, J. Hao, and M. Cocivera, J. Lumin. **99**, 349 (2002).
- <sup>6</sup>M. Moszynski, M. Balcerzyk, and M. Kapusta, IEEE Trans. Nucl. Sci. **52**, 3124 (2005).
- <sup>7</sup>P. Kozma and P. Koma, Radiat. Phys. Chem. **71**, 705 (2004).
- <sup>8</sup>F. Danevich, A. Georgadze, and V. Kobychov, AIP Conf. Proc. **785**, 87 (2005).
- <sup>9</sup>M. Lammers, G. Blasse, and D. Robertson, Phys. Status Solidi A **63**, 569 (1981).
- <sup>10</sup>M. Treadaway and R. Powell, Prog. Low Temp. Phys. **11**, 862 (1975).
- <sup>11</sup>F. Wen, X. Zhao, H. Huo, J. Chen, E. Lin, and J. Zhang, Mater. Lett. **55**, 152 (2002).
- <sup>12</sup>H. Meyssamy and K. Riwozki, Adv. Mater. **11**, 840 (1999).
- <sup>13</sup>R. Meltzer, S. Feofilov, and B. Tissue, Phys. Rev. B **60**, R14012 (1999).
- <sup>14</sup>H. Song, B. Chen, H. Peng, and J. Zhang, Appl. Phys. Lett. **81**, 1776 (2002).
- <sup>15</sup>J. Shin, G. Hoven, and A. Polman, Appl. Phys. Lett. **66**, 2379 (1995).
- <sup>16</sup>M. Waite and A. Vecht, Appl. Phys. Lett. **19**, 471 (1971).
- <sup>17</sup>H. Song, L. Yu, S. Lu, T. Wang, Z. Liu, and L. Yang, Appl. Phys. Lett. **85**, 470 (2004).
- <sup>18</sup>L. Yu, H. Song, S. Lu, Z. Liu, and L. Yang, Chem. Phys. Lett. **399**, 384 (2004).
- <sup>19</sup>C. Wu, W. Qin, G. Qin, D. Zhao, J. Zhang, and S. Huang, Appl. Phys. Lett. **82**, 520 (2003).
- <sup>20</sup>C. Jia, L. Sun, F. Luo, X. Jiang, L. Wei, and C. Yan, Appl. Phys. Lett. **84**, 5305 (2004).
- <sup>21</sup>V. Mikhailik, H. Kraus, and D. Wahl, Phys. Rev. B **69**, 205110 (2004).
- <sup>22</sup>M. Daturi, L. Savary, G. Costentin, and J. Lavalley, Catal. Today **61**, 231 (2000).
- <sup>23</sup>E. Elsts and U. Rogulis, Phys. Status Solidi C **2**, 69 (2005).
- <sup>24</sup>S. Shigeo and M. William, Phosphor Handbook (CRC Press, Washington, DC, 1998).
- <sup>25</sup>B. Li, Y. Liu, Z. Zhi, D. Shen, Y. Lu, J. Zhang, and X. Fan, J. Cryst. Growth **240**, 479 (2002).
- <sup>26</sup>H. Peng, H. Song, B. Chen, S. Lu, and S. Huang, Chem. Phys. Lett. **370**, 485 (2003).